ACS Photonics

Review

pubs.acs.org/journal/apchd5

Ultrafast Nonlinear Plasmonic Spectroscopy: From Dipole Nanoantennas to Complex Hybrid Plasmonic Structures

Bernd Metzger, Mario Hentschel, and Harald Giessen*

4th Physics Institute and Research Center SCoPE, University of Stuttgart, Pfaffenwaldring 57, 70569 Stuttgart, Germany

ABSTRACT: The key property of metal nanostructures is their unique ability to channel far-field radiation to subwavelength dimensions. The resulting strongly confined and enhanced electromagnetic fields boost nonlinear optical effects at the nanoscale. In this Review article we highlight and summarize the recent most important investigations and advances in the field of "nonlinear plasmonic spectroscopy", and we present results of second- and third-harmonic spectroscopy experiments of plasmonic nanoantenna arrays that consist of different unit cell elements, ranging from dipole nanoantennas to complex hybrid plasmonic structures. The experiments on dipole nanoantennas show that nonlinear optical processes can be enhanced by plasmonic resonances either at the fundamental laser wavelength or at the spectral position of the harmonic signal. Furthermore, we investigate the quadrupolar third-harmonic response of dolmen-type plasmonic Fano structures and find that the third-harmonic polarization field of the quadrupolar mode does not radiate to the far-field due to destructive interference. Finally, we incorporate indium tin oxide nanocrystals into the hot-spot of plasmonic gap-antennas and find a doubling of the third-harmonic response of the hybrid antennas when compared to bare gold gap-antennas. The experimental results of the nanoantenna arrays can be modeled and understood using a classical model of anharmonic oscillators and are supported by finite element simulations. Parts of this Review article are based on previous publications.[1−4]

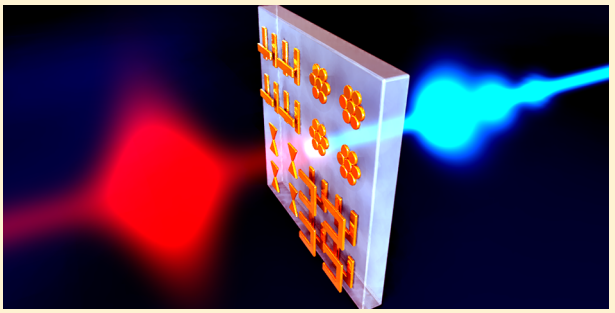

KEYWORDS: *ultrafast spectroscopy, nonlinear optics, plasmonics, second-harmonic generation, third-harmonic generation*

The unique feature of plasmonic nanoantennas is to squeeze far-field radiation to subwavelength dimensions and vice versa.[5−8] At the origin are collective oscillations of the conduction electrons that can be excited in metal nanostructures by propagating electromagnetic waves.[9−12] Associated with the light confinement is a strong enhancement of the surrounding electromagnetic fields and an exceptionally high polarization on the surface of the metal nanoantennas. Hence, by focusing ultrashort laser pulses on a metal nanoantenna electromagnetic energy can be concentrated in time and space, and the resulting strongly enhanced fields are highly interesting to boost nonlinear optical effects at the nanoscale.[13,14]

Nonlinear optical phenomena often are described by and arise from additional terms in the electric polarization, which show a superlinear dependence on the local electric fields. Consequently, at large light intensities when these additional contributions to the electric polarization gain importance, electromagnetic waves effectively start to interact beyond linear interference. In second-harmonic (SH) generation for example, to name a prominent nonlinear optical effect, two photons excite an electron to a virtual state, which subsequently coherently emits a photon of twice the incoming energy.

The high electric field strength associated with plasmonic resonances stimulated researchers early on to study nonlinear optical phenomena in differently shaped metal nanostructures. Among others, pioneering work was carried out in 2006 by Klein and co-workers, who investigated the SH response of arrays of plasmonic split ring resonators (SRRs).[15] Already one year earlier, Lippitz et al. studied the third-harmonic (TH) generation from single gold nanoparticles.[16]

In the following years scientists made use of different promising concepts to further boost the efficiency of nonlinear optical effects. A widely studied method for example uses doubly resonant plasmonic antennas to enhance the SH response.[17] These plasmonic nanostructures exhibit a plasmonic resonance not only at the fundamental exciting laser wavelength but also at the wavelength of the generated nonlinear signal. The concept has been proven to efficiently boost the overall conversion efficiency of nonlinear optical effects in numerous publications.[4,18−22] Furthermore, doubly or even multiple resonant antennas can also be used to amplify the fields of two or several different incoming frequencies for boosting for example nonlinear optical four-wave mixing.[23]

Another approach to enhance the conversion efficiency of nonlinear optical effects is based on the fact that the effective intensity enhancement typically scales quadratically with the lifetime of the associated plasmonic resonances.[3,24,25] Hence, researchers aimed for plasmonic modes that exhibit a longer lifetime or equivalently a narrower linewidth, since this

Special Issue: Nonlinear and Ultrafast Nanophotonics

Received: October 14, 2015
Published: July 28, 2016

DOI: 10.1021/acsphotonics.5b00587
ACS Photonics 2016, 3, 1336−1350

dramatically influences and enhances the efficiency of nonlinear optical effects. Most prominently, plasmonic Fano resonances have been utilized to achieve the reduction in linewidth,[2,26,27] even in combination with the aforementioned doubly resonant nanoantenna design.[28,29]

Beyond that it has been envisioned that the strong local electric fields in the vicinity of plasmonic nanostructures can be utilized to boost the efficiency of nonlinear optical effects in semiconducting or dielectric materials. There are few examples where researchers unambiguously observed a nonlinear optical signal contribution from a nonplasmonic material driven by the enhanced electric near-field of plasmonic nanostructures. Already in 2006, K. Chen et al. observed plasmon-enhanced SH generation from ionic self-assembled multilayer films.[30] Furthermore, in 2009 Niesler et al. fabricated SRR arrays with varying spatial orientation on a GaAs substrate and in dependence on the SRR orientation they were able to observe and drive different elements of the second-order susceptibility tensor of the GaAs.[31] Noteworthy is also the work by J. Lee and co-workers, who observed a strong nonlinear response by coupling plasmonic metasurfaces to intersubband transitions of multi-quantum-well semiconductor heterostructures.[32]

In several other experiments researchers incorporated nonlinear dielectrics into the hot-spot of plasmonic gap-antennas. Thorough investigations revealed that the incorporation of the dielectrics can lead to an enhancement of the nonlinear response; however, this enhancement is not caused by the optical nonlinearity of the dielectrics, but has to be attributed to an increased field enhancement that predominantly drives the optical nonlinearity of the metals.[3,20]

In parallel to the efforts for boosting the efficiency of nonlinear optical effects researchers also aimed for a better understanding of the microscopic origin of the nonlinear response. In particular, the influence of the symmetry of the nanostructure geometry on the SH response has been studied in detail, most remarkably by the group of M. Kauranen.[33,34] While in most cases these symmetry selection rules predict the measured results in a convincing and precise fashion, in some cases they fail. In particular, inversion symmetric dipole nanoantennas have been found to exhibit a strong SH response,[4,20] although for these structures SH generation should be forbidden by symmetry in dipole approximation. In other studies Linden et al. investigated the influence of the lattice constant of arrays of SRRs on the SH response and found that collective effects in the lattice strongly influence the second-harmonic response.[35] Furthermore, tailoring the geometry of a plasmonic metamaterial allowed researchers to realize a material with either a focusing or a defocusing Kerr-type nonlinearity.[36] Very recently also the nonlinear response of chiral plasmonic structures and metasurfaces has been investigated,[37,38] and nonlinear plasmonic elements have been introduced for efficient terahertz generation[39] and as sensors in refractive index sensing.[40]

In this review we summarize our most important recent results on nonlinear optical spectroscopy of plasmonic nanostructure arrays, ranging from dipole nanoantennas to complex hybrid plasmonic structures.

First, we study the nonlinear optical response of rod-type gold and aluminum nanoantenna arrays. Such dipole nanoantennas can be tailored to exhibit localized surface plasmon resonances (LSPR) either at the fundamental laser wavelength or at the wavelength of a desired nonlinear harmonic signal.[41,42] We find that both configurations allow boosting nonlinear optical processes such as SH or TH generation significantly.[1,4,13,43]

Second, we investigate the TH mechanism of complex plasmonic Fano structures.[2] In a plasmonic system a Fano resonance originates from the coupling of a bright and a dark mode. The increased lifetime of the dark mode offers the possibility to further increase the efficiency of nonlinear optical effects.[26,44] In the investigated dolmen-type structures the Fano resonance is realized by coupling a dark quadrupolar mode to a bright dipole antenna.[45−48] We find that as in the case of the fundamental field the quadrupolar mode does not radiate nonlinear signals to the far-field due to destructive interference. However, by symmetry breaking the quadrupolar mode of the dolmen-type structures can be rendered partially bright, i.e., more dipole-like, so that TH energy is efficiently emitting to the far-field. An understanding of the corresponding linear and nonlinear measurements can be obtained by performing electrodynamic finite element simulations and by modeling the plasmonic modes using an anharmonic coupled oscillator model that utilizes a complex coupling coefficient that accounts for the retarded interaction between the coupled plasmonic modes.

Finally, we incorporate indium tin oxide (ITO) nanocrystals as a nonlinear dielectric material into the hot-spot of plasmonic gap-antennas and investigate whether the strongly confined and enhanced electromagnetic fields allow for boosting nonlinear optical effects within the volume of the dielectric material. We find that the TH response of corresponding hybrid ITO nanocrystal-incorporated plasmonic gap-antennas exhibits a two-times enhanced efficiency for TH generation when compared to identical plasmonic gap-antennas without ITO nanocrystals. Thorough experiments and a comparison with simulations reveal that the source of the enhancement of the hybrid antennas can fully be attributed to an increased plasmonic near-field that is caused by the presence of the dielectric ITO nanocrystals. However, this field predominantly drives the optical nonlinearity of the gold gap-antennas rather than the third-order susceptibility of the ITO nanocrystals.

EXPERIMENTAL SETUP

In classical nonlinear optical experiments typically bulk crystals such as lithium niobate or beta barium borate are used for frequency conversion. These crystals are usually driven far off-resonance to prevent absorption that would decrease the overall conversion efficiency, which could lead to optical damage. Therefore, the nonlinear coefficients that describe the efficiency for frequency conversion are nearly frequency independent over a large spectral range. In contrast, metal nanostructures exhibit strong LSPRs in the visible and the near-infrared, and hence nonlinear optics of plasmonic nanostructures are *resonant nonlinear optics*. As a consequence, the nonlinear optical properties of metal nanoantennas are highly frequency dependent and strongly depend on their linear optical response. Therefore, it is necessary to perform spectrally resolved nonlinear optical spectroscopy to ensure a resonant excitation of the nanostructures and to determine the spectral position of highest conversion efficiency.

Consequently, we use a sophisticated experimental setup that enables nonlinear optical spectroscopy over a large spectral range. The setup is schematically depicted in Figure 1. We utilize a home-built Yb:KGW solitary mode-locked oscillator emitting 175 fs laser pulses at a repetition rate of 44 MHz and a central wavelength of 1030 nm.[49] The oscillator laser pulses are

DOI: 10.1021/acsphotonics.5b00587
ACS Photonics 2016, 3, 1336−1350

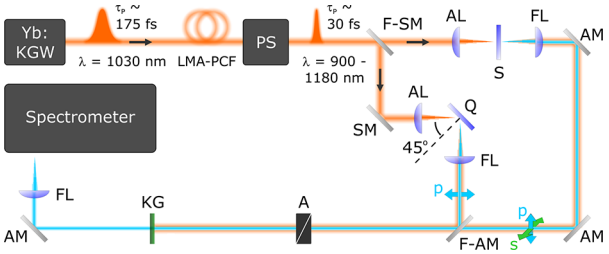

Figure 1. Experimental setup for measuring polarization-resolved SH and TH spectra. LMA-PCF: large mode area photonic crystal fiber, PS: pulse shaper, F: flip mirror, SM: silver mirror, AM: aluminum mirror, AL: achromatic lens, FL: fused silica lens, S: sample, Q: quartz crystal, A: analyzer, KG: KG filters. Reprinted with permission from *Nano Lett.* **2015**, *15*, 3917−3922. Copyright 2015 American Chemical Society.

sent into a nonlinear photonic crystal fiber for spectral broadening and subsequently into a 4f pulse shaper for amplitude and phase modulation. This setup allows generation of shaped sub-30 fs laser pulses tunable from 900 to 1180 nm.[50]

For nonlinear spectroscopy experiments of plasmonic nanostructure arrays the laser pulses from the pulse shaper are focused onto the sample under normal incidence using a 75 mm focal length achromatic lens with an average power between about 10 and 25 mW. This leads to a beam diameter in the focus of about 50 μm and to peak intensities on the order of about 1 GW/cm^2. Subsequently, we collimate the nonlinear signals radiated in the forward direction using a fused silica lens, send the signals through an analyzer, filter the fundamental laser light, and measure the nonlinear signals with a Peltier-cooled CCD camera attached to a spectrometer. After the measurements we integrate the measured nonlinear spectra over all wavelength components to obtain a scalar value describing the signal intensity. Lastly, to eliminate the influence of the wavelength dependence of the optical components in the experimental setup and to account for different average powers of the laser source at different spectral positions, we normalize all nonlinear signals from the nanostructures to reference nonlinear signals. In the case of SH spectroscopy we use a flip mirror to focus the laser pulses by an identical lens in p-polarization onto a birefringent quartz crystal under an angle of incidence of 45°, generating a reference SH signal;[51] see Figure 1. In the case of TH spectroscopy the reference TH signals are generated either at the bare fused silica substrate[1] or at a 20 nm thick gold film.[2]

PLASMONIC DIPOLE NANOANTENNAS

The first plasmonic nanostructure arrays we discuss here consist of gold nanoantennas that exhibit a dipolar LSPR for light polarized along their long axis. The nanoantenna lengths are chosen such that their plasmon resonances approximately coincide with the fundamental laser wavelength. Consequently, the absorbance of fundamental laser light at frequency ω is resonantly enhanced by the plasmon resonances, which is sketched by a corresponding energy level diagram in Figure 2.

The investigated nanoantenna arrays with an area of 100 × 100 μm^2 are fabricated by standard electron beam lithography on Suprasil (Heraeus) substrates. The individual rod-type antennas show a nominal height and width of 40 and 60 nm, respectively, and the antenna length is tuned among different arrays between 200 and 250 nm. The grating period in both directions is 500 nm. Figure 2 shows scanning electron

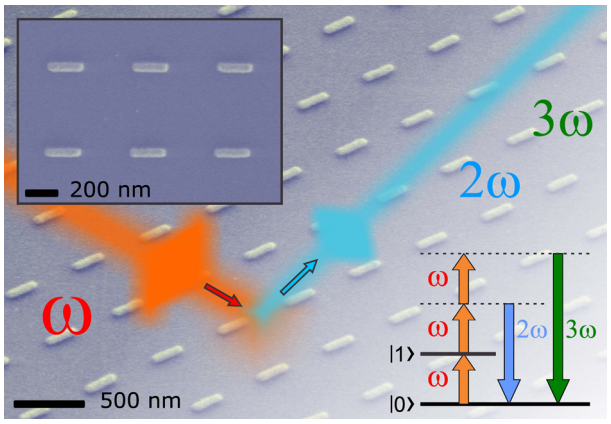

Figure 2. Schematic illustration of SH and TH generation in Au-nanoantenna arrays that are resonant to the laser at frequency ω. The background and the inset show tilted scanning electron micrographs of an investigated Au-nanoantenna array.

microscope (SEM) images of one particular antenna array with an antenna length of about 225 nm.

Before the nonlinear spectroscopy experiments of the antenna arrays we measured their linear extinction spectra. The measured extinction spectrum $\alpha_z = -\ln(T)$ of one antenna array is depicted in Figure 3a, displaying an LSPR at a central wavelength of about 1025 nm. In Figure 3a we also plot a shaped laser spectrum with a Gaussian-like spectral shape with a central wavelength of 1000 nm and a bandwidth of 45 nm. This bandwidth corresponds to a Fourier-limited pulse duration of about 30 fs. The corresponding measured nonlinear spectrum of the radiated nonlinear signals after focusing this

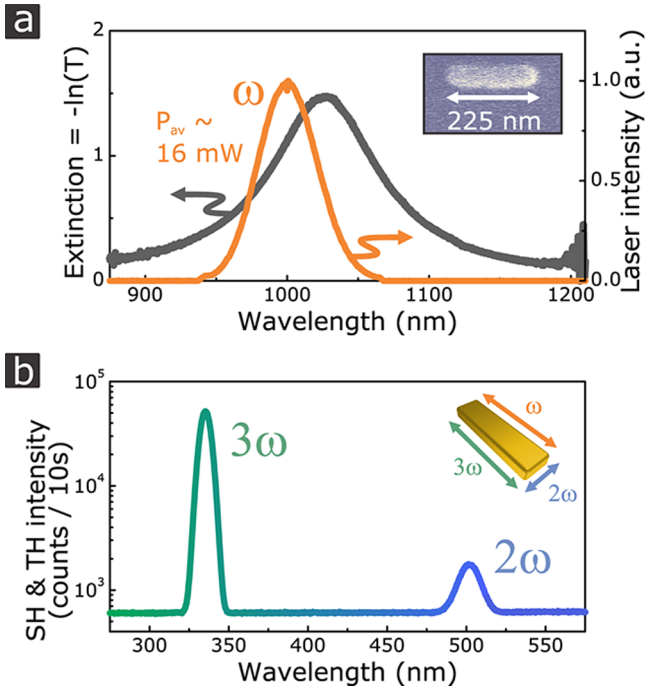

Figure 3. (a) Measured extinction spectrum (black) of a gold nanoantenna array with an antenna length of about 225 nm as well as a measured Gaussian laser spectrum (orange) at a central wavelength of 1000 nm, which is focused on the nanoantenna array with an average power of 16 mW. (b) Corresponding measured SH and TH signals, which occur at a wavelength of 500 and 333 nm, respectively.

DOI: 10.1021/acsphotonics.5b00587
ACS Photonics 2016, 3, 1336−1350

laser spectrum under normal incidence and polarized along the antenna axes on the nanoantenna array is shown in Figure 3b. We observe two peaks, namely, at two times and three times the incoming frequency, at a wavelength of 500 and 333 nm, respectively, which correspond to the generated SH and TH signals.

It is quite unexpected that we observe a SH signal in the experiment. The dipole nanoantennas are inversion symmetric, and hence, second-order nonlinear optical effects such as SH generation should be forbidden in dipole approximation. The microscopic origin of the radiated SH signals of inversion symmetric plasmonic structures could be the surface of the metal nanostructures or the substrate, which breaks the symmetry along the propagation direction. Also higher order tensor elements, such as the magnetic dipole or the electric quadrupole, might contribute to the SH response; however, this is still under discussion.

When analyzing the polarization state of the nonlinear signals, we find that the generated TH in Figure 3b exhibits the same polarization state as the incoming laser light and, hence, is polarized parallel to the plasmonic nanoantennas. In contrast, the polarization of the SH signals is mainly oriented perpendicular to the antennas. However, also a weak contribution polarized parallel to the antennas of the generated SH could be detected.

In order to unambiguously prove that the measured nonlinear signals originate from two-photon and three-photon processes, we measured the SH and TH signal intensity in dependence on the average input power on a gold nanoantenna array and on the bare substrate. The corresponding results are depicted in Figure 4.

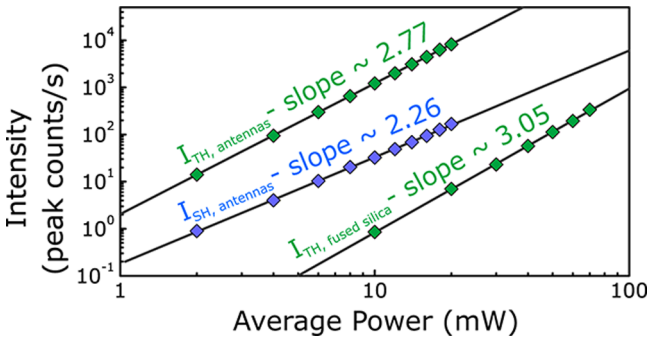

Figure 4. Measured peak intensities of SH and TH signals plotted over the incident average power generated on a gold nanoantenna array with an antenna length of 225 nm and measured TH peak intensities generated on a fused silica substrate.

In the case of the TH power dependence of the bare substrate we find an increase that almost perfectly follows the expected power of 3 dependence. In the case of the nonlinear signals that are generated at the plasmonic nanoantenna array we find a slope of about 2.26 and 2.77 for SH and TH generation, respectively. Hence, both signals are proven to be of nonlinear origin; however, they are found to deviate quite remarkably from the expected power of 2 and 3 behavior. In the case of SH generation the larger slope might indicate that higher order tensor elements contribute to the SH response of the nanoantennas, while in the case of TH generation intensity-dependent losses seem to limit the TH conversion efficiency. Remarkably, at a typical average power of about 10 mW the SH signal intensity of the nanoantenna array is about an order of magnitude stronger than the TH of the fused silica substrate, but it is also about an order of magnitude weaker than the TH of the nanoantenna array.

THIRD-HARMONIC RESPONSE OF GOLD NANOANTENNAS RESONANT TO THE LASER WAVELENGTH

To determine the spectral dependence of TH generation on the plasmonic nanoantenna arrays, we measured the linear extinction spectra and the wavelength-dependent TH intensities on five different antenna arrays, where we increased the length of the individual gold antennas from 200 nm to 245 nm. These antenna arrays are located on three different samples. Hence, the width, the height, and the quality of the antennas might differ slightly, even though they are nominally fabricated with equal parameters. The change in antenna length leads mainly to a shift of the fundamental LSPR from about 970 to about 1100 nm.

The results of these measurements are depicted in Figure 5. The measured TH intensities (green, diamonds) are plotted over the fundamental laser wavelength together with the corresponding linear extinction spectra (black) for increasing nanoantenna length from top to bottom. Every data point in the TH intensity corresponds to a measured TH spectrum, which was integrated over all wavelength components and was normalized to the TH of the bare substrate. We find that when the nanoantennas are resonantly excited, the TH intensity can be up to 3 orders of magnitude larger than that of the bare substrate. Furthermore, the peak of the TH generation intensity is always located close to and slightly red-shifted with respect to the maximum of the linear extinction spectrum.

Anharmonic Oscillator Model. The behavior of the TH response of the plasmonic nanoantenna arrays can be modeled with an anharmonic oscillator model.[13,43] We treat the particle plasmon as a classical harmonic oscillator with a small perturbation that is proportional to $x^3(t)$:

$$\ddot{x} + 2\gamma\dot{x} + \omega_0^2 x + ax^3 = -\frac{e}{m}E(t) \tag{1}$$

where $x(t)$ denotes the oscillator amplitude, γ describes its damping, ω_0 is the resonance frequency, a is a small perturbation parameter and describes the strength of the TH, e corresponds to the charge, m is the mass of the oscillator, and $E(t)$ is the incident electric field amplitude of the laser pulses.

The solution to this differential equation can be obtained using perturbation theory. We express $x(t)$ in a power series for the perturbation parameter a as $x(t) = x^{(0)}(t) + ax^{(1)}(t) + O(a^2)$. The first term $x^{(0)}(t)$ corresponds to the unperturbed solution, while $x^{(1)}(t)$ is the first-order correction that oscillates at the TH frequency. Since the solution of $x^{(0)}(t)$ is required to calculate $x^{(1)}(t)$, we first solve the unperturbed harmonic oscillation by Fourier transformation. The solution is given by

$$x^{(0)}(\omega) = -\frac{e}{m}g(\omega)\,E(\omega) \tag{2}$$

where $g(\omega) = -(\omega^2 - \omega_0^2 + 2i\gamma\omega)^{-1}$ is the linear response function of an oscillator. Furthermore, we relate the linear response function $g(\omega)$ to an effective linear optical susceptibility $\chi^{(1)}(\omega) = e^2\, n/\epsilon_0 m\, g(\omega)$, where n corresponds to the number density of the plasmonic oscillators, and we derive an expression for the linear extinction spectrum $\alpha(\omega)$:

DOI: 10.1021/acsphotonics.5b00587
ACS Photonics 2016, 3, 1336−1350

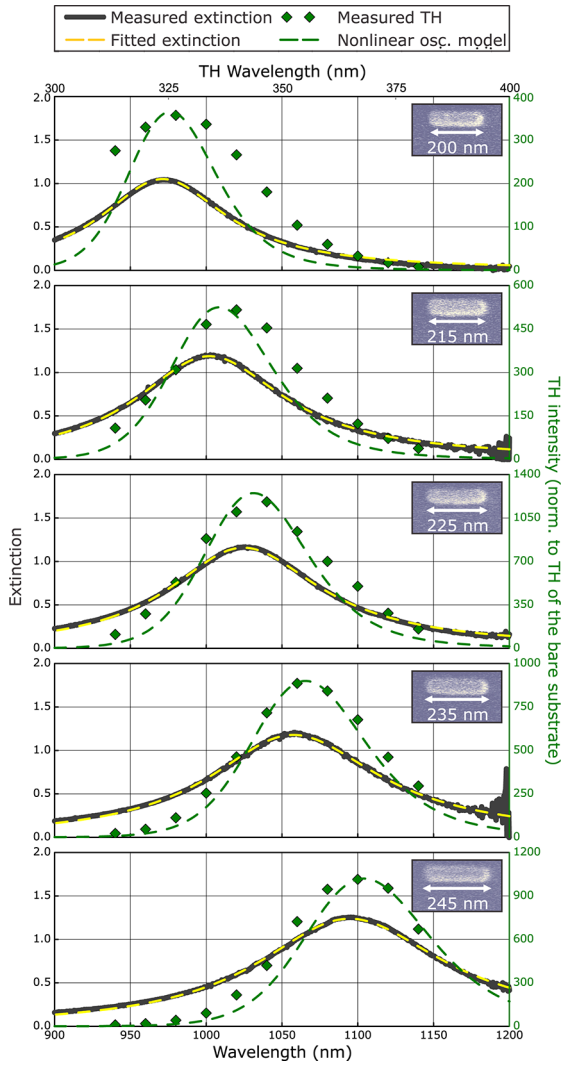

Figure 5. Measured and modeled TH intensities with respect to the linear extinction spectra plotted over the fundamental laser wavelength. The top axis shows the TH wavelength. From top to bottom the length of the antennas increases from 200 nm to 245 nm. The insets show colored scanning electron micrographs of a single antenna element of the corresponding nanoantenna array. Reprinted with permission from *Opt. Lett.* **2012**, 37, 4741−4743. Copyright 2012 Optical Society of America.

$$\alpha(\omega) = \frac{\omega}{c}\mathrm{Im}\{\chi^{(1)}(\omega)\} \tag{3}$$

$$= \frac{e^2 n}{\epsilon_0 c m} \frac{\gamma\omega^2}{(\omega^2 - \omega_0^2)^2 + 4\gamma^2\omega^2} \tag{4}$$

The extinction spectrum $\alpha(\omega)$, comprising absorbance and scattering, allows for quantification of the interaction of the light field with the plasmonic antennas. Hence, expression 4 can be used as a fit function for the measured extinction spectra. The fits of the extinction spectra are shown in Figure 5 (yellow, dashed). From the fits it is possible to extract the parameters γ and ω_0, which are the main parameters we need to calculate the unperturbed solution $x^{(0)}(t)$.

Subsequently, the solution for $x^{(1)}(\omega)$ can be calculated as $x^{(1)}(\omega) = -g(\omega)\,\mathcal{F}\{(x^{(0)}(t))^3\}$, where $\mathcal{F}$ denotes a Fourier transform. The TH intensity $I_{\mathrm{TH}}(\omega)$ radiated to the far-field is calculated as[52]

$$I_{\mathrm{TH}}(\omega) \propto |E_{\mathrm{TH}}(\omega)|^2 \propto |\omega x^{(1)}(\omega)|^2 \tag{5}$$

If this model is used to describe the measured TH intensities, we obtain the green dashed curves in Figure 5. The anharmonic oscillator model explains the experimental behavior including the slight red-shift of the TH intensites with respect to the linear extinction spectra quantitatively.

The physical origin of this shift is that the TH generation is most efficient when the plasmon oscillator amplitude $|x^{(0)}(\omega)|$ is at its maximum value. The peak of the amplitude however is red-shifted with respect to the linear extinction spectrum due to the damped nature of the plasmon oscillator.[53] The plasmon oscillator amplitude $|x^{(0)}(\omega)|$ does not peak at the resonance frequency ω_0, but at the red-shifted near-field resonance frequency $\omega_{\mathrm{NF}} = \sqrt{\omega_0^2 - 2\gamma^2}$.[54] In contrast, the far-field extinction spectrum $\alpha(\omega)$ of eq 4 peaks independent of the damping constant γ at the resonance frequency ω_0. Therefore, the TH intensity peaks are slightly red-shifted with respect to the linear extinction spectrum.

The only free parameter in this model is the perturbation parameter a, into which information about the intrinsic bare gold nonlinearity enters. In our case it acts as a scaling parameter for the absolute TH intensities and is for all five antenna arrays individually scaled so that the simulation fits the measured data points best. Yet, the complete wavelength dependence of the TH response is well predicted by the model.

Linewidth, Resonance Position, and Their Influence on the Near-Field Enhancement. In the previous section we have seen that the anharmonic oscillator is able to describe the lineshape of the linear and the TH optical response of plasmonic nanoantennas that are resonant to the laser wavelength quite well. However, we did not use the oscillator model to predict the relative efficiency of TH generation between different nanonantenna arrays, but rather scaled the modeled TH curves to the measured ones.

However, the oscillator model can also provide estimates on the overall efficiency of nonlinear optical processes, at least to some extent, which we illustrate in the following. In the oscillator model the source term for nonlinear optical effects is the plasmon oscillator amplitude $x^{(0)}$, which is proportional to the effective field enhancement of the plasmonic nanoantennas.

Here, we consider the absolute value of the plasmon oscillator amplitude $|x^{(0)}(\omega)| = e/m|g(\omega)\,E(\omega)|$. For continuous wave excitation with $E(t) = E_0\,e^{-i\omega t}$ we obtain in the frequency domain

$$\left|x^{(0)}(\omega)\right| = \frac{2\pi e E_0}{m} \frac{1}{\sqrt{(\omega^2 - \omega_0^2)^2 + 4\gamma^2\omega^2}} \tag{6}$$

We have seen that the oscillator amplitude peaks at the red-shifted near-field resonance frequency $\omega_{\mathrm{NF}} = \sqrt{\omega_0^2 - 2\gamma^2}$.[53] Hence, its peak value is given by

$$\left|x^{(0)}(\omega_{\mathrm{NF}})\right| = \frac{2\pi e E_0}{m} \frac{1}{2\gamma\sqrt{\omega_0^2 - \gamma^2}} \tag{7}$$

$$\approx \frac{2\pi e E_0}{m} \frac{1}{2\gamma\omega_0} \propto \frac{1}{\gamma\omega_0} \tag{8}$$

where we used the approximation $\gamma \ll \omega_0$, which is often well fulfilled for plasmonic oscillators. We find the oscillator

DOI: 10.1021/acsphotonics.5b00587
ACS Photonics 2016, 3, 1336−1350

amplitude, or equivalently the electric near-field enhancement, to be inversely proportional to the resonance frequency ω_0 and the damping constant γ.

At first glance it might appear unexpected that the resonance position ω_0 influences the absolute value of the near-field enhancement. However, the resonance frequency ω_0 is directly related to the restoring force of a classical oscillator, and hence it is intuitive that a lower resonance frequency ω_0, which corresponds to a reduced restoring force, leads to a higher oscillator amplitude.

Furthermore, the amplitude of the oscillation increases with decreasing damping γ. Hence, a long lifetime τ or equivalently a narrow linewidth of the plasmon resonances also leads to higher field enhancement.[24,42]

Finally, nonlinear optical effects scale with higher powers of the field enhancement. For example the TH intensity scales with the sixth power of the plasmon oscillator amplitude. Hence, the TH intensity critically depends on these quantities and increases with decreasing ω_0 and with $1/\gamma^6$.[13]

It is important to note that the harmonic oscillator is a purely classical model and cannot replace a full quantitative electrodynamic simulation. In real systems a number of effects take place simultaneously that are not accounted for by the oscillator model. However, the simple model provides an intuitive picture of the enhancement of nonlinear optical processes in plasmonic nanostructures.

SECOND-HARMONIC RESPONSE OF AL-NANOANTENNAS RESONANT TO THE SECOND-HARMONIC WAVELENGTH

The nanostructures that are investigated in the following are again dipole nanoantennas. However, this time they are not designed to exhibit plasmonic resonances in the spectral range of the fundamental wavelength, but at the SH wavelength. Consequently, the emission of a SH polarization field to the far-field can be resonantly enhanced; see Figure 6.

In order to experimentally investigate the emission enhancement by plasmonic nanoantennas for SH generation, we fabricated aluminum nanoantenna arrays with an area of 100 × 100 μm^2 on a fused silica substrate. In contrast to gold, which is hampered by interband absorptions in the visible spectral range,[55] aluminum nanostructures can exhibit well-modulated plasmonic modes in our SH wavelength range between 450 and 570 nm,[56] and small interband absorption effects are seen only around 800 nm.[57] The height and width of the individual rod-type nanoantennas are 50 and 60 nm, respectively, and their length is varied from 120 to 150 nm. The lattice constant in both directions is 300 nm; corresponding scanning electron micrographs can be seen in Figure 6.

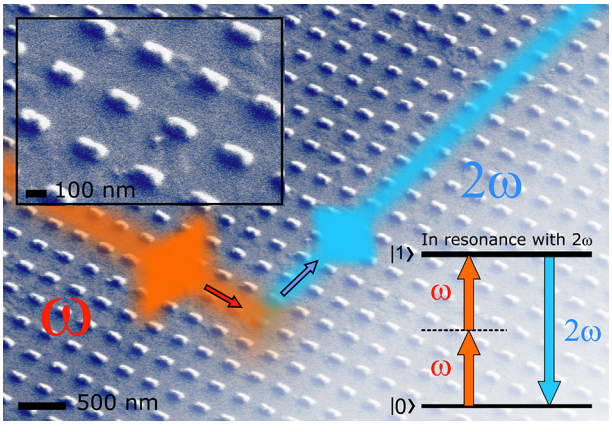

Figure 6. Illustration of SH spectroscopy of Al-nanoantennas that are resonant to the SH wavelength. The background and the inset show tilted scanning electron micrographs of the investigated sample. Reprinted with permission from *Nano Lett.* **2015**, *15*, 3917−3922. Copyright 2015 American Chemical Society.

As before, in advance of SH spectroscopy experiments we measured linear optical spectra of the nanoantenna arrays under normal incidence using a linearly p- or s-polarized white light source. Beyond their common meaning, p- and s-polarization here denote the polarization direction parallel and perpendicular to the nanoantenna long axis, respectively. For reflection measurements we utilized a 100 nm thick aluminum film for the reference reflection. In Figure 7 an exemplary reflectance spectrum (black) measured in p-polarization of a nanoantenna array is shown, which exhibits a longitudinal LSPR at a central wavelength of about 520 nm. The measured s-polarized reflectance spectra exhibit no distinct features in the considered spectral range. Figure 7 also depicts a measured laser spectrum (red) at a central wavelength of 1000 nm and a corresponding measured SH spectrum (blue) at a wavelength of 500 nm. The red- and the blue-shaded areas indicate the tuning range of the central wavelength of our laser source and the SH signals, respectively.

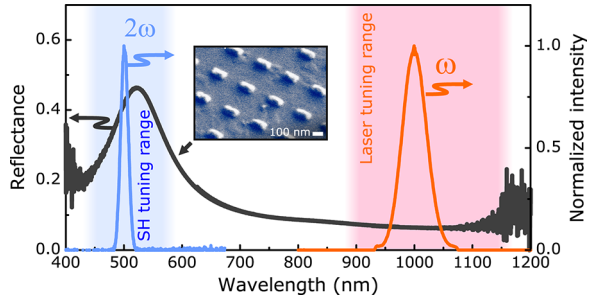

Figure 7. Exemplary measured laser spectrum (red) and its corresponding measured SH spectrum (blue) with respect to the measured reflectance spectrum of an aluminum nanoantenna array (black). The inset shows a tilted scanning electron micrograph of the corresponding nanoantenna array. Reprinted with permission from *Nano Lett.* **2015**, *15*, 3917−3922. Copyright 2015 American Chemical Society.

The experimental results of SH spectroscopy experiments for excitation under normal incidence are shown in Figure 8a for various nanoantenna arrays with different nanoantenna lengths l increasing from top to bottom. A number of important observations can be made: First, for increasing antenna length l the LSPRs red-shift as expected from the linear reflectance spectra (black). Second, together with the red-shift, the linewidth of the plasmon resonances increases monotonically, which can most likely be attributed to an increased coupling between the different antenna elements in an entire nanoantenna array.[35,58] Third, the p-polarized SH signals (blue) almost follow the reflectance spectra of the nanoantenna arrays; however, there is an obvious trend for the peaks of the SH intensities to be slightly blue-shifted with respect to the peaks of the linear reflectance spectra. Fourth, we also observe comparably weak s-polarized SH signals (green), increasing toward shorter wavelength.

DOI: 10.1021/acsphotonics.5b00587
ACS Photonics 2016, 3, 1336−1350

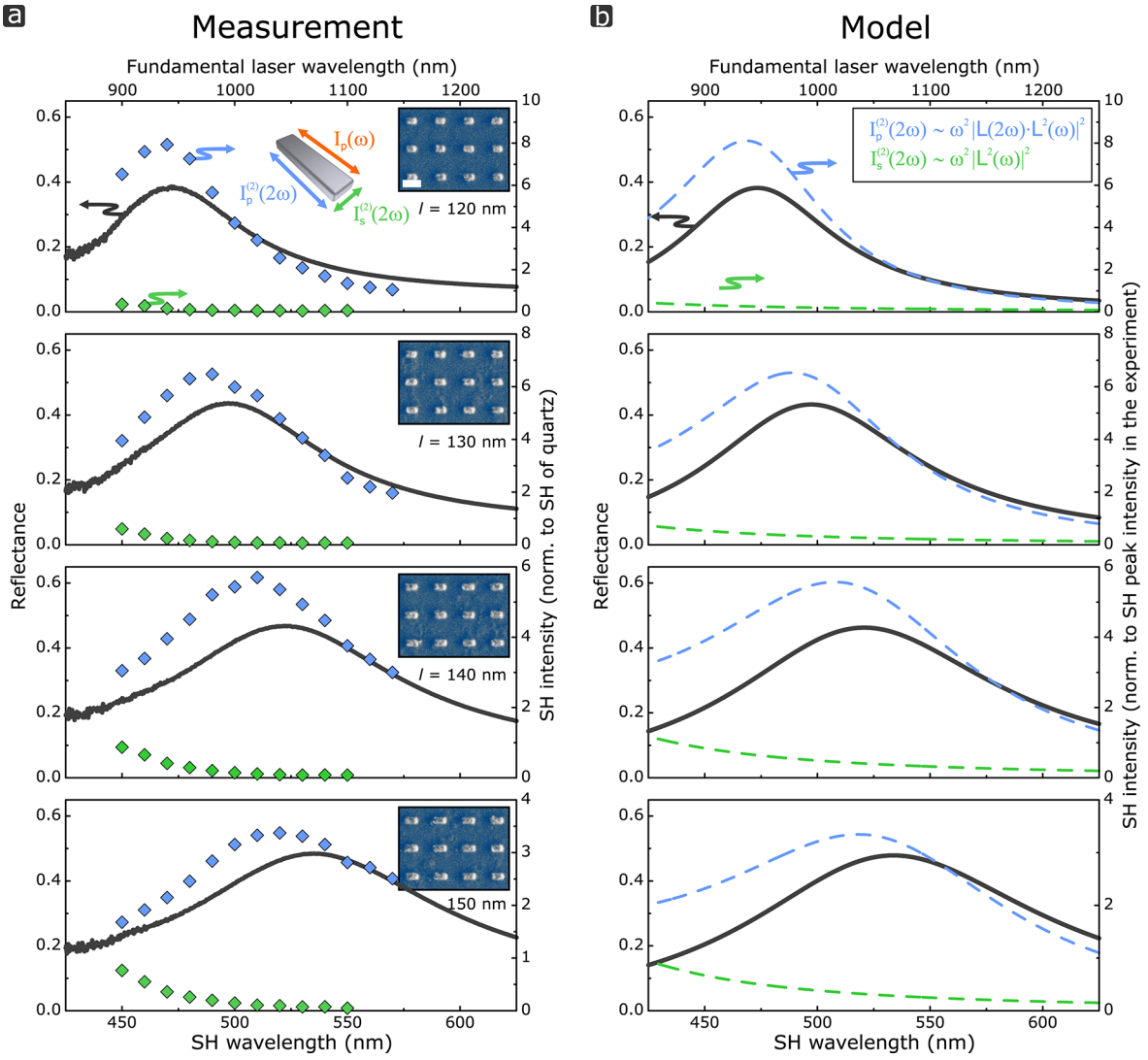

Figure 8. Measured (a) and modeled (b) polarization-resolved SH spectra together with the corresponding reflectance spectra of four aluminum nanoantenna arrays with different nanoantenna length l increasing from top to bottom from about 120 to 150 nm plotted over the SH wavelength. The top axis shows the corresponding fundamental laser wavelength. The insets show corresponding scanning electron micrographs. The scale bar is 200 nm. Reprinted with permission from *Nano Lett.* **2015**, *15*, 3917−3922. Copyright 2015 American Chemical Society.

In order to gain more insight into the nonlinear optical processes and to understand the spectral behavior of the SH intensities, the plasmonic resonances are modeled in a quite similar fashion to that in the previous section using a phenomenological field enhancement factor, $L(\omega)$, that accounts for the field enhancement caused by the plasmonic resonances at the fundamental field and at the SH field. For a single plasmonic resonance this field enhancement factor $L(\omega)$ can be approximated by a Lorentzian, and in the radiated SH amplitudes it enters quadratically at the fundamental field and linearly in the SH field.[4,59]

The results of the modeled s- and p-polarized SH intensities are depicted together with the modeled reflectance spectra in Figure 8b. First of all, the enhanced radiation efficiency for the p-polarized SH intensity (blue) is well described by the model, as is the slight blue-shift of its peak position. Moreover, also the increase of the s-polarized SH intensity (green) toward shorter wavelength is reproduced. Admittedly, the relative SH signal strength between the four nanoantenna arrays is not well described by the model. In the measurement the p-polarized SH intensities are found to increase toward shorter nanoantenna length, which can be attributed to the previously mentioned narrowing of the resonance linewidth.[35] This trend can also qualitatively be confirmed and understood by the field enhancement factors, which increase in amplitude for decreasing resonance linewidth. However, the quantitative agreement of the relative SH intensities of the four nanoantenna arrays between the measurement and the model is limited. Therefore, the modeled p-polarized SH intensities have been independently scaled so that the modeled peak values agree with the measured SH peak value of the corresponding nanoantenna array. However, the relative SH signal strengths between the two SH polarization components of one nanoantenna array are well approximated by the model, since the s- and p-polarized SH intensities have been scaled with the same factor, respectively.

The results of the modeling allow understanding the details of the SH spectra: Although the nanoantenna arrays are resonant to the SH wavelength, the tails of the resonances stretch all the way to the fundamental laser wavelength. Hence,

DOI: 10.1021/acsphotonics.5b00587
ACS Photonics 2016, 3, 1336−1350

the absorbance of the fundamental laser light is increased when the laser is tuned toward shorter wavelength, which leads to the increase of the s-polarized SH intensity. The blue-shift of the p-polarized SH intensity is closely related to this phenomenon. The radiation efficiency for the p-polarized SH signals that are enhanced by the plasmon resonance peaks at the far-field resonance frequency ω_0; however, due to the increased absorption for the incoming laser radiation tuned toward shorter wavelengths, the overall p-polarized SH intensity curve shifts to the blue.

To summarize this section, plasmonic nanoantennas that exhibit plasmonic resonances at the SH wavelength allow efficiently boosting the emission of SH signals to the far-field. In the case of dipole nanoantennas the peak of the SH generation is located slightly blue-shifted with respect to the linear optical spectra, which can be explained by a model that accounts for the almost off-resonant absorption at the fundamental wavelength and the resonant emission process at the SH wavelength.[4]

PLASMONIC FANO STRUCTURES

So far, we investigated plasmonic nanostructures that exhibit Lorentzian-like plasmonic modes. However, there is another prominent type of resonance, which can be formed when dark and bright plasmonic modes are coupled together, referred to as plasmonic Fano resonances. Due to their reduced linewidth, they are considered highly attractive for enhancing nonlinear optical effects at the nanoscale.[26,45−48]

In the following we study the linear and TH response of dolmen-type plasmonic Fano structures, as shown in Figure 9.

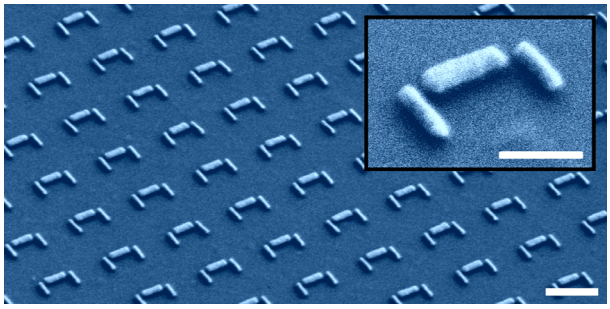

Figure 9. Tilted SEM images of dolmen-type plasmonic Fano structures. The length and width of the dipole antenna are 220 and 70 nm. The length and width of the quadrupole antennas are 190 and 50 nm. The gap distance between the dipole and the quadrupole is about 50 nm, and the structure height is 60 nm. The lattice constants of the nanostructure arrays are 600 and 700 nm perpendicular and parallel to the dipole rod, respectively. The scale bars are 500 and 200 nm in the overview and the inset, respectively. Reprinted with permission from *ACS Photonics* **2014**, *1*, 471−476. Copyright 2014 American Chemical Society.

In these nanostructures a dark plasmonic mode is realized by two parallel dipole nanoantennas, which together form a quadrupolar mode. This dark quadrupolar mode is coupled to a bright dipole antenna. The interference of the two modes leads to the typical Fano lineshape in the linear spectrum, which is characterized by a spectrally narrow transmittance window within a broad absorbance peak. In particular, we investigate the TH response of the quadrupolar mode and find that as in the case of the fundamental field the TH polarization field of the quadrupolar mode does not radiate to the far-field due to destructive interference. Beyond that, we extend the anharmonic oscillator to a coupled anharmonic oscillator model that takes retardation between the two plasmonic modes into account by using a complex coupling coefficient.[60] This model allows us to describe and understand the linear and the nonlinear spectra in a descriptive fashion.

The first experimental results of linear and TH spectroscopy measurements of a dolmen-type plasmonic Fano structure array are shown in Figure 10a. Throughout these experiments the

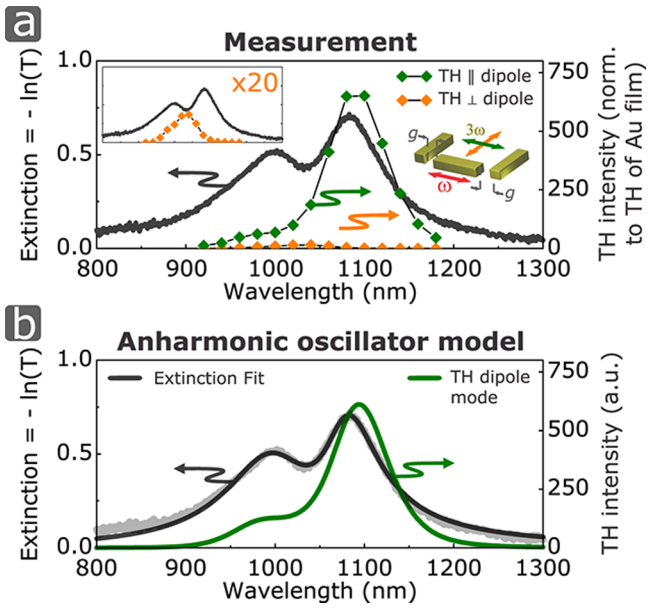

Figure 10. Measured (a) and modeled (b) TH spectra plotted together with the corresponding linear extinction spectrum of a dolmen-type plasmonic Fano structure array with a gap distance g of about 50 nm. Reprinted with permission from ACS Photonics **2014**, *1*, 471−476. Copyright 2014 American Chemical Society.

polarization of the incoming laser light is oriented along the dipole antenna. We find the TH that is polarized parallel to the dipole to peak close to the low-energy peak of the Fano resonance (green diamonds). Neither in the Fano resonance dip nor at the high-energy peak is strong TH emission observed. Furthermore, perpendicular to the dipole, only very weak TH emission can be detected (orange diamonds). The inset shows the perpendicularly polarized TH in a magnified fashion, which we find to peak close to the Fano resonance dip.

In order to unravel the underlying physical mechanisms, we describe the dipole and the quadrupole mode as classical harmonic coupled oscillators with a small cubic perturbation, which accounts for the TH response:[13,47,61−63]

$$\ddot{x}_\mathrm{d} + 2\gamma_\mathrm{d}\dot{x}_\mathrm{d} + \omega_\mathrm{d}^2 x_\mathrm{d} - \kappa x_\mathrm{q} + a x_\mathrm{d}^3 = -\frac{e}{m}E(t) \tag{9}$$

$$\ddot{x}_\mathrm{q} + 2\gamma_\mathrm{q}\dot{x}_\mathrm{q} + \omega_\mathrm{q}^2 x_\mathrm{q} - \kappa x_\mathrm{d} + a x_\mathrm{q}^3 = 0 \tag{10}$$

where the indices j = d, q represent the dipole and the quadrupole mode, respectively, $x_j(t)$ are the oscillator amplitudes, γ_j are the damping constants, ω_j denote the resonance frequencies, κ describes the coupling strength, a is a perturbation parameter, which determines the strength of the TH, e is the charge of the dipole mode, m is its mass, and $E(t)$ is the electric field amplitude of the incident laser pulses.

DOI: 10.1021/acsphotonics.5b00587
ACS Photonics 2016, 3, 1336−1350

As a consequence of the relatively large gap distance g of 50 nm of the structures and the resulting retardation between the modes, we utilize a complex coupling coefficient $\kappa = |\kappa| e^{i\phi}$.[60] The origin of this complex-valued coupling coefficient will be discussed further below. The solution of the coupled differential equations again can be obtained in the frequency domain using perturbation theory. The unperturbed solution for the amplitudes $x_j^{(0)}(\omega)$ then follow from a matrix inversion:

$$\begin{bmatrix} x_d^{(0)} \\ x_q^{(0)} \end{bmatrix} = -\frac{e}{m}\frac{1}{1-\kappa^2 g_d g_q}\begin{bmatrix} g_d & \kappa g_d g_q \\ \kappa g_d g_q & g_q \end{bmatrix}\begin{bmatrix} E(\omega) \\ 0 \end{bmatrix} \tag{11}$$

where $g_j(\omega) = -[\omega^2 - \omega_j^2 + 2i\gamma_j\omega]^{-1}$ denote the linear response functions of the two oscillators. From the solution a formula for the extinction spectrum $\alpha(\omega)$ for light polarized along the dipole can be derived;[47,60] compare formula 3:

$$\alpha(\omega) = \frac{e^2 n}{\epsilon_0 m}\frac{\omega}{c}\mathrm{Im}\left[\frac{g_d}{1-\kappa^2 g_d g_q}\right] \tag{12}$$

Fitting of the measured linear extinction spectra with the expression for $\alpha(\omega)$ yields the linear optical properties (ω_j, γ_j, κ) of the coupled oscillator system. Subsequently, the solution in first-order perturbation $x_j^{(1)}(\omega)$, which describes the TH response, can be calculated as $x_j^{(1)}(\omega) \propto \mathcal{F}\{(x_j^{(0)}(t))^3\}$. Consequently, the expression for $x_d^{(1)}(\omega)$ allows calculating the radiated TH from the dipole antenna.[1,43,64]

The results of the anharmonic coupled oscillator model are depicted in Figure 10b. The TH radiated from the dipole (green) is shown together with the fitted linear extinction spectrum (black). The model describes all features of the radiated TH intensity polarized parallel to the dipole. In particular the peak position of the TH is found close to the low-energy peak. Hence, the TH parallel to the dipole is completely described by the TH of the dipole mode. The TH from the mode of the quadrupole rods is predicted by the model to peak between the Fano resonance dip and the low-energy peak (not shown). This spectral position suggests that the weak TH measured perpendicular to the dipole stems from the quadrupole rods.

To examine the microscopic source of the quadrupolar TH in more detail, we perform FEM simulations (Comsol Multiphysics) of the dolmen-type structures. In the simulations the structures are defined with the dimensions given in Figure 9 and are positioned on a substrate with a constant refractive index of $n = 1.5$, and for the optical properties of gold we use the data of Johnson and Christy.[55] The TH polarization $\mathbf{P}_{TH}(\mathbf{r})$ at each spatial coordinate $\mathbf{r}$ can be obtained from the linear polarization $\mathbf{P}(\mathbf{r})$ via

$$\mathbf{P}_{TH} \propto \chi_{Au}^{(3)}\mathbf{E}^3 \propto [\chi_{Au}^{(1)}]^3\mathbf{E}^3 \propto \mathbf{P}^3 \tag{13}$$

where $\mathbf{E}$ corresponds to the complex local electric field amplitude and $\chi_{Au}^{(1)}$ and $\chi_{Au}^{(3)}$ are the first- and third-order susceptibilities of bare gold, respectively. After the second approximate sign, we used the classical expression for the third-order susceptibility, after which it is proportional to the third power of the first-order susceptibility.[13]

The simulated x- and y-polarized TH polarization field distributions are shown in Figure 11. We find the x-polarized TH polarization field predominantly located in the dipole antenna. This confirms that the TH polarized parallel to the dipole is originating from the dipole mode. Furthermore, the y-polarized TH polarization field is equally distributed in the quadrupolar rods. However, as a consequence of the out-of-phase oscillation of the quadrupolar mode, this TH polarization field does not radiate efficiently to the far-field due to destructive interference.

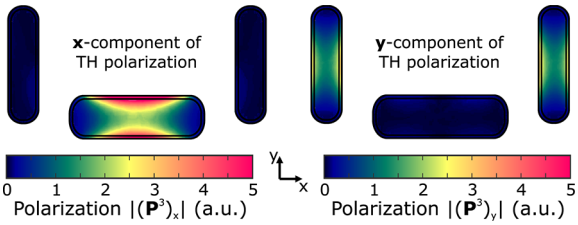

Figure 11. Simulated field distributions of the absolute value of the x-component (left) and the y-component (right) of the TH polarization field in dolmen-type gold nanostructures with a gap distance of 50 nm, each plotted at their corresponding spectral peak position. Reprinted with permission from *ACS Photonics* **2014**, *1*, 471−476. Copyright 2014 American Chemical Society.

In order to test this hypothesis and to further elaborate on the origin of the perpendicularly polarized TH, we now shift the dipole of the structures in small steps from its center position closer to one of the quadrupole wires; see the SEM images in Figure 12. The introduced asymmetry leads to an unequal coupling between the dipole rod and the perpendicularly oriented rods. Hence, the two quadrupole rods are now

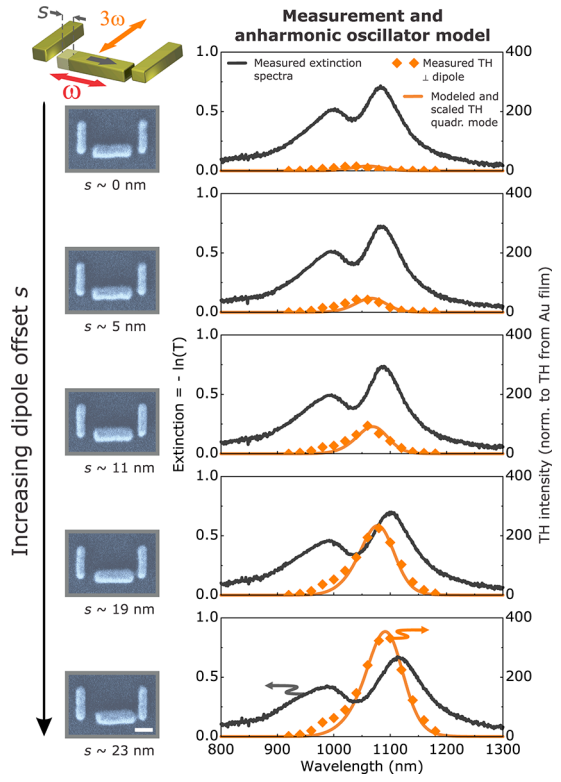

Figure 12. Measured and modeled TH spectra polarized perpendicular to the dipole antenna for increasing dipole offset s together with corresponding linear extinction spectra from top to bottom. On the left SEM images are depicted, respectively. The scale bar is 100 nm. Reprinted with permission from *ACS Photonics* **2014**, *1*, 471−476. Copyright 2014 American Chemical Society.

DOI: 10.1021/acsphotonics.5b00587
ACS Photonics 2016, 3, 1336−1350

excited with different strength and phase (due to the distance-dependent retarded coupling).

The corresponding TH spectroscopy measurements are depicted in Figure 12, where the measured TH signals polarized perpendicular to the dipole (orange, diamonds) together with the measured linear extinction spectra (black) are shown, with increasing dipole offset s from top to bottom. We find a monotonic increase of the TH emission with increasing dipole offset s. As before, we fitted the linear extinction spectra with the coupled oscillator model and calculated subsequently the displacement $x_q^{(1)}(\omega)$ describing the TH of the mode of the quadrupole rods; see Figure 12 (orange, lines). It is noteworthy that only in the fully symmetric case is the plasmonic mode of the quadrupole rods a pure quadrupolar mode. As soon as the symmetry is broken by displacing the dipole wire, the excited mode in the quadrupole rods x_q will be a superposition of the dark quadrupolar mode and a more dipole-like contribution. Importantly, the oscillator model does not include information about how efficient the mode of the quadrupole rods x_q radiates TH light into the far-field. In contrast to the spectral behavior the absolute far-field TH strength is a parameter that cannot be predicted by the model. Therefore, the modeled TH spectra are scaled with respect to amplitude to the measured TH data points. Nevertheless, the spectral behavior and the peak position of the TH are very well predicted by the model.

We also simulated the TH polarization-field distribution of a symmetry-broken dolmen-type structure with an exemplary dipole offset s of 30 nm, which is shown in Figure 13. As before,

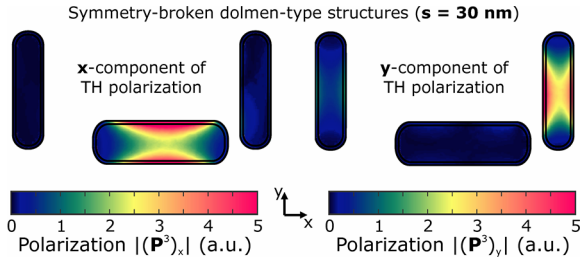

Figure 13. Simulated field distributions of the absolute value of the x-component (left) and the y-component (right) of the TH polarization field in asymmetric dolmen-type Fano structures (s = 30 nm), each plotted at their corresponding spectral peak position. Reprinted with permission from *ACS Photonics* **2014**, *1*, 471−476. Copyright 2014 American Chemical Society.

the x-polarized TH polarization field is located in the dipole antenna. However, the y-polarized TH polarization field is no longer equally distributed in both quadrupolar bars, but is predominantly located in the quadrupolar bar that features a smaller gap distance with respect to the dipole antenna.

We conclude that for the symmetric structure the TH polarization field of the mode of the quadrupole rods interferes destructively in the far-field due to the out-of-phase oscillation in the two quadrupole wires. For increasing dipole offset s the unequal excitation of the quadrupole wires leads to reduced destructive interference and hence to an efficient radiation of the TH light to the far-field.

Complex Coupling Coefficient in Coupled Plasmonic Systems. In order to describe the linear and the TH response of dolmen-type plasmonic Fano structures in the previous section within the framework of a coupled oscillator model, we needed to implement a complex coupling coefficient:

$$\kappa = |\kappa| e^{i\phi} \quad (14)$$

to account for the retarded interaction between the plasmonic modes. Since we did not discuss the origin of this complex coupling coefficient in detail, we further elaborate on this.

We fabricated another series of gold dolmen-type nanostructure arrays with the same geometrical parameters as given in Figure 9; however, for this sample we varied the gap distance g from about 20 nm to 100 nm in steps of 10 nm, and for comparison we also fabricated a dipole antenna array, which exhibits the same lattice constant as the dolmen-type nanostructures.

For excitation along the dipole antenna of the dolmen-type structures we measured the transmittance spectra T and the reflectance spectra R and calculated via $T + R + A = 1$ the corresponding absorbance spectra A. The resulting absorbance spectra are depicted in Figure 14 for decreasing gap distance g

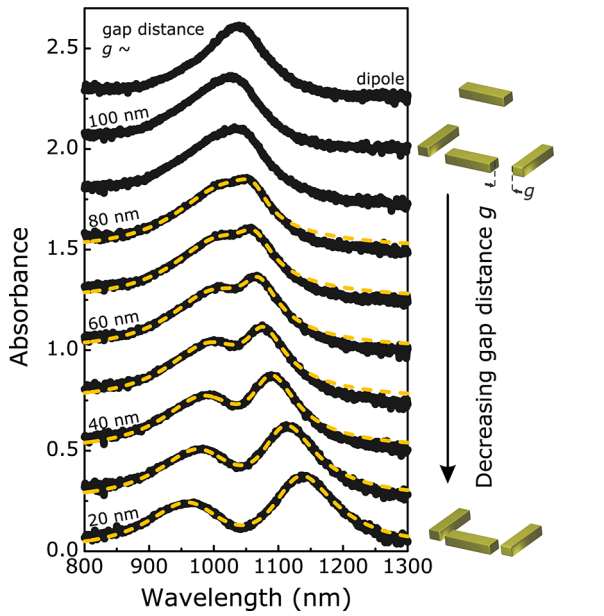

Figure 14. Measured (black, line) and fitted (yellow, dashed) absorbance spectra of plasmonic dolmen-type nanostructure arrays for different values of the gap distance g, decreasing from top to bottom from about 100 nm to about 20 nm. The topmost spectrum corresponds to the absorbance of a dipole antenna array, which lacks the quadrupole rods.

from top to bottom. For increasing coupling, i.e., decreasing gap distance, we observe as expected a more pronounced splitting of the Fano resonance peaks.

We fitted the linear optical absorbance spectra with eq 12 of the coupled oscillator model for the seven smallest gap distances of the sample. For larger gap distances than about 80 nm the fitting of the absorbance spectra becomes highly ambiguous due to the weak coupling between the plasmonic modes. The free parameters in the fitting are the two resonance frequencies ω_d and ω_q, the damping constants γ_d and γ_q, the coupling coefficient κ, and an overall amplitude. We find that the absorbance spectra cannot be fitted using a purely real coupling coefficient κ, in particular in the case of the larger gap distances. However, by implementing a complex coupling coefficient $\kappa = |\kappa| e^{i\phi}$ the absorbance spectra can be fitted very well.[60] In Figure 14 the fits of the absorbance spectra are shown together with the measured absorbance spectra.

DOI: 10.1021/acsphotonics.5b00587
ACS Photonics 2016, 3, 1336−1350

From the fits it is possible to extract the absolute value |κ| and the phase ϕ of the complex coupling coefficient κ, which are displayed in Figure 15 with respect to the gap distance g. As

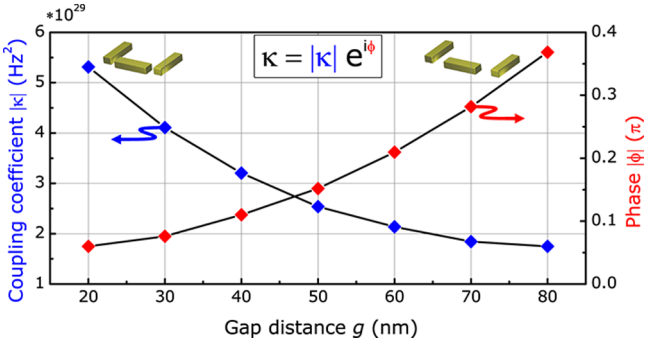

Figure 15. Absolute value |κ| and phase ϕ of the complex coupling coefficient κ for different values of the gap distance g in plasmonic dolmen-type Fano structures, which have been determined by fitting of the measured absorbance spectra with eq 12.

expected, we find a monotonic decrease of the absolute value |κ| of the coupling coefficient for increasing gap distance g. This circumstance is caused by a reduced near-field coupling for larger distances of the plasmonic nanorods.

In addition to the absolute value |κ| of the coupling coefficient we show its phase ϕ, which is found to increase monotonically in its absolute value for increasing gap distance g. As mentioned at the beginning, the reason for the increase of the phase for a larger gap distance is the retarded interaction between the gold nanorods. The effect of an electromagnetic interaction can spread maximally with the speed of light, which leads to a noninstantaneous coupling of the two plasmonic modes.

To summarize, the interaction between plasmonic nanoantennas that are separated by several tens of nanometers is noninstantaneous due to the retardation of light. This circumstance can be described in the oscillator model by the implementation of a complex coupling coefficient $\kappa = |\kappa| e^{i\phi}$.[60]

ITO NANOCRYSTAL-INCORPORATED PLASMONIC GAP-ANTENNAS

In this last section we incorporate nonlinear dielectric materials into the hot-spot of plasmonic gap-antennas, to make use of the field enhancement effect in the gap region of the antennas and to boost the optical nonlinearity of the dielectric material.

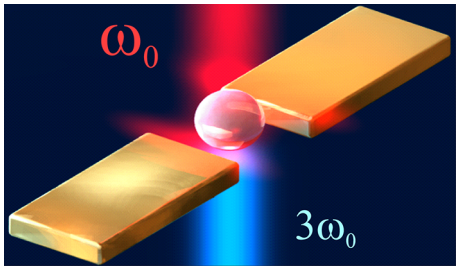

Figure 16. Illustration of TH generation in hybrid ITO nanocrystal-incorporated plasmonic gap-antennas. Reprinted with permission from *Nano Lett.* **2014**, *14*, 2867−2872. Copyright 2014 American Chemical Society.

First, we demonstrate the fabrication of hybrid ITO nanocrystal-incorporated plasmonic gap-antennas using a two-step electron beam lithography process. Second, we experimentally investigate the hybrid nanostructure arrays by means of TH spectroscopy and observe doubling of the TH response of the hybrid system when comparing to the TH response of an identical bare plasmonic gap-antenna array, without ITO nanocrystals. Third, we identify the origin of the TH signal enhancement, which is mainly related to changes in the linear optical properties and the lifetime of the plasmonic antenna resonances.

In the experiments we utilize arrays of dimer nanoantennas consisting of two identical gold rods separated by a small gap. Illuminating the nanostructure arrays with electromagnetic plane waves polarized along the long axis of the gap-antennas excites the hybridized symmetric plasmonic mode, located in the near-infrared spectral region at about 1000 nm. To estimate the electric field enhancement $|\mathbf{E}|/|\mathbf{E}_0|$ associated with this plasmonic mode, we perform finite element simulations of the structures, where $\mathbf{E}$ and $\mathbf{E}_0$ are defined as the local electric field amplitude and the incoming electric far-field amplitude, respectively. For the simulations we utilize a commercial software package (Comsol Multiphysics). Therein, the structures are defined on a substrate with a constant refractive index of n = 1.5, and for the optical properties of gold we use the data of Johnson and Christy.[55] Figure 17 shows the electric

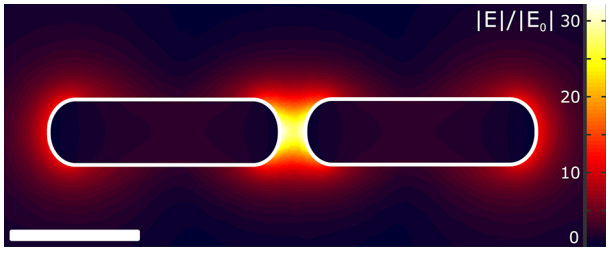

Figure 17. Simulation of the electric near-field enhancement $|\mathbf{E}|/|\mathbf{E}_0|$ of a plasmonic gap-antenna. The field distribution is shown for the plane symmetrically cutting the antenna and for resonant excitation. The scale bar corresponds to 100 nm. Reprinted with permission from *Nano Lett.* **2014**, *14*, 2867−2872. Copyright 2014 American Chemical Society.

field enhancement $|\mathbf{E}|/|\mathbf{E}_0|$ for resonant plane wave excitation of a plasmonic gap-antenna. As expected, the strongest electric field enhancement of about 20 to 30 is observed in the gap region of the dimer nanoantenna, which is commonly referred to as the antenna "hot-spot".[65] This hot-spot is generally expected to be the major source of any nonlinear signal and is in particular the ideal position for a selective incorporation of a nonlinear dielectric.[8,25]

In order to experimentally study a system made of hybrid nanoparticle-incorporated plasmonic gap-antennas, we developed a process for the selective filling of the antenna gaps with different kinds of nanoparticles. The fabrication of the hybrid nanostructure arrays works via a two-step electron beam exposure[66] and a subsequent so-called squeegee process.[67,68] In a first step the nanoantennas as well as alignment marks are defined in a double-layer poly(methyl methacrylate) (PMMA) resist on a fused silica substrate (Suprasil, Heraeus), followed by the evaporation of a 2 nm Cr adhesion layer and a 40 nm gold layer and the subsequent lift-off of the resist. Afterward, the sample is once again coated with a double layer of PMMA

DOI: 10.1021/acsphotonics.5b00587
ACS Photonics 2016, 3, 1336−1350

resist, and the alignment marks are used to selectively open resist apertures on top of the nanoantenna gaps. Subsequently, the nanocrystals can be transferred into the apertures from solution. In our case monodisperse ITO nanocrystals have been synthesized according to literature methods,[69] resulting in a mean crystal diameter of 6 nm, suspended in hexane. A droplet of the concentrated nanocrystal−hexane solution is deposited onto the resist and swept across the sample surface by a cut piece of polydimethylsiloxane (PDMS). The nanocrystals are dragged along with the meniscus of the slowly evaporating hexane solution and deposited into the resist openings.[68] Once the hexane is nearly fully evaporated, the remaining nanocrystals are dragged to the rim of the substrate and away from the gold nanostructures in order to prevent clustering in the structured areas. Subsequently, the sample is placed top-down on additional glass slides in an acetone beaker to remove the PMMA resist mask and the excess nanocrystals. The final nanoantenna arrays have a size of 90 × 90 μm^2, with an excellent filling ratio of the antenna feed gaps; see scanning electron micrographs in Figure 18.

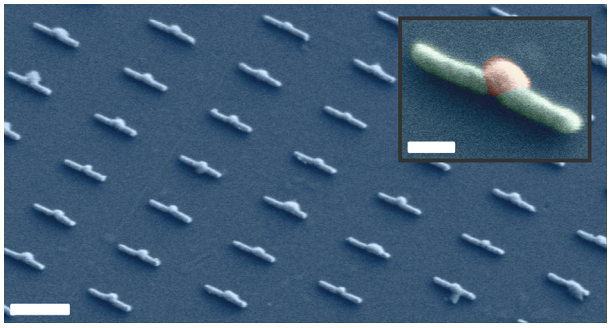

Figure 18. Colored SEM image of a hybrid ITO nanocrystal-incorporated plasmonic gap-antenna array. The inset shows an SEM of a single antenna element. The individual gap-antenna elements consist of two identical gold rods, with a height, a width, and a length of about 40, 50, and 180 nm, respectively. The gap distance is about 20 nm. The scale bar is 500 nm in the overview and 100 nm in the inset, respectively. Reprinted with permission from *Nano Lett.* **2014**, *14*, 2867−2872. Copyright 2014 American Chemical Society.

The incorporation of the high refractive index ITO nanocrystals into the hot-spot of the gold gap-antennas influences the plasmonic mode of the nanoantennas, since these are highly sensitive to changes in the dielectric environment. In particular, the resonance frequency ω_0 of the plasmonic mode shifts to lower frequencies due to the increase in the outer effective dielectric constant.

In Figure 19a the results of TH spectroscopy experiments for one exemplary bare (green) and one hybrid (orange) antenna array are shown. The solid lines correspond to measured linear extinction spectra of the antenna arrays, whereas the data points (diamonds) represent normalized TH intensities. The linear extinction spectrum of the bare gap-antenna array (green) is characterized by a single Lorentzian peak associated with its plasmon resonance at around 1025 nm. As reported in earlier work,[1,53,70] we find the peak of the TH conversion efficiency (green, diamonds) close yet slightly red-shifted with respect to the peak of its far-field extinction spectrum. As mentioned above, the incorporation of the ITO nanocrystals leads to a significant red-shift of the extinction peak by about 45 nm. The origin of the red-shift is the increase of the dielectric constant ϵ_m of the environment, which changes in the gap region, that is,

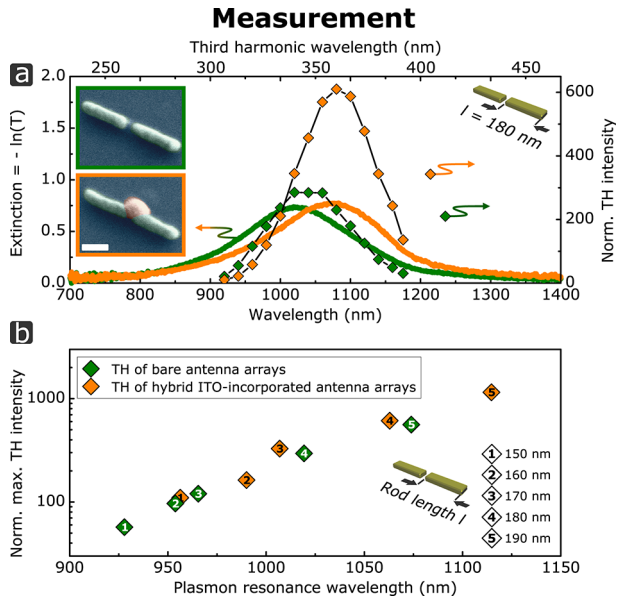

Figure 19. (a) TH spectroscopy of bare (green) and hybrid ITO nanocrystal-incorporated (orange) plasmonic gap-antenna arrays, with an antenna length l of about 180 nm. The lines correspond to measured extinction spectra; the data points are measured TH intensities plotted over the fundamental excitation wavelength. The top axis shows the corresponding TH wavelength. (b) Maximum of the measured TH intensities of different bare (green) and ITO nanocrystal-incorporated (orange) gap-antenna arrays with different antenna length l plotted over their corresponding plasmon resonance wavelength. Data points with identical labeling correspond to an equal antenna length l, which is given in the right corner of the graph. Reprinted with permission from *Nano Lett.* **2014**, *14*, 2867−2872. Copyright 2014 American Chemical Society.

the ITO volume from $\epsilon_{m,AIR} = 1$ of air to about $\epsilon_{m,ITO} \approx 2.9$ of the ITO.[71] Consequently, the peak of the TH conversion efficiency (orange, diamonds) shifts together with the linear spectrum to longer wavelengths by about the same value. The maximum TH conversion efficiency is about a factor of 2 larger when compared to that of the bare gap-antenna arrays.

In order to further investigate the role of the ITO nanocrystals in the measured enhancement of the TH conversion efficiency, we tune the spectral characteristics of the gap-antennas by varying the length l of the two gold rods from about 150 nm to about 190 nm, in a step size of 10 nm. As before, we measured the TH spectra of the bare as well as the hybrid ITO nanocrystal-incorporated antenna arrays. The measured linear and TH signal spectra exhibit very similar behavior to the exemplary one shown in Figure 19a. For clarity, in Figure 19b we plot only the maximum TH signal strength for each antenna array versus the spectral position of its plasmonic resonance (green: bare; orange: nanocrystal-incorporated). We observe a monotonic increase of the TH intensity radiated from all measured antenna arrays when plotted over their corresponding plasmon resonance wavelength. In particular, we find that the TH signal increases by about an order of magnitude in the considered wavelength range. Most importantly, the TH maxima of the hybrid nanocrystal-incorporated gap-antenna arrays and the bare antenna arrays follow the same trend, not only qualitatively but also quantitatively. The measured data suggest that only the spectral position of the plasmonic resonance determines the maximum TH signal. In contrast, if there is a significant contribution of

DOI: 10.1021/acsphotonics.5b00587
ACS Photonics 2016, 3, 1336−1350

the ITO nanocrystals to the overall TH signal, the bare and the ITO nanocrystal-incorporated antenna arrays should form two distinct subsets in Figure 19b, with the latter having a higher overall TH signal. The observation that they form a single indistinguishable set is a strong indication that a contribution of the ITO nanocrystals to the overall TH intensity is not the main reason for the observed increased TH conversion efficiency.

As we have seen above, the linear optical properties of a plasmonic system have a crucial influence on its nonlinear optical response. In particular, the spectral position of the plasmon resonance frequency ω_0 and the damping constant γ are of crucial importance.[1,35,43] When analyzing the plasmon resonances, we find a monotonic decrease in the resonance linewidth for increasing resonance wavelength, independent of whether there are ITO nanocrystals incorporated into the antenna gaps or not.[3]

Thus, for the bare and the hybrid nanostructure arrays the increase in the TH signal strength is mainly related to a decrease of the resonance frequency ω_0 and a decrease in the resonance linewidth, i.e., the damping constant γ, which lead to an enhanced polarization field of the red-shifted plasmon resonances and therefore to increased generation of TH light in the gold volume of the plasmonic gap-antennas.

To summarize, we incorporated ITO nanocrystals into the hot-spot of plasmonic gap-antennas and observed an enhancement of the TH signals radiated from the hybrid gap-antenna arrays by about a factor of 2 when comparing them to the TH signals of identical bare plasmonic gap-antenna arrays. A close study revealed that the enhanced TH signal strength is mainly related to changes in the linear optical properties of the respective antenna arrays. The incorporation of the ITO nanocrystals leads to a red-shift of the plasmon resonance and therefore to a decrease of the resonance frequency ω_0 and the resonance linewidth γ. Both decreasing quantities increase the polarization-field amplitude of the plasmonic antennas and ultimately lead to the observed increase in the TH signal strength. Furthermore, the TH signal is found to be nearly exclusively generated in the gold volume, which also can be confirmed by corresponding finite element simulations of the nanostructures,[3] and not inside the ITO nanocrystals as reported in another publication.[72] While the exact experimental conditions in the other publication might have been quite different from our experiments, and hence, it might be possible that they indeed observed a significant TH signal contribution from the ITO nanoparticles, our work shows that it is highly important to take changes in the field enhancement carefully into account when varying the dielectric environment of plasmonic nanoantennas to unambiguously determine the origin of the nonlinear response.[20]

SUMMARY AND OUTLOOK

To summarize, localized surface plasmon resonances of plasmonic nanoantennas allow enhancing nonlinear optical effects at the nanoscale. The resulting nonlinear conversion efficiencies surpass the efficiency of nonlinear optical effects in dielectrics in comparable nanoscale volumes by orders of magnitude. Most importantly, the plasmonic elements are efficient frequency converters only when driven at resonance, either at the fundamental wavelength or at the harmonic signal.

We showed that the plasmonic resonances of dipole nanoantennas that are located either at the fundamental wavelength or at the wavelength of a nonlinear signal allow boosting second- or third-harmonic generation significantly. Furthermore, we investigated the quadrupolar third-harmonic response of dolmen-type plasmonic Fano structures and found that the third-harmonic polarization field of the quadrupolar mode does not radiate to the far-field due to destructive interference. However, symmetry breaking in the nanostructures renders the quadrupolar mode more dipole-like, which allows the efficient transfer of third-harmonic energy to the far-field. Lastly, we investigated the third-harmonic response of hybrid indium tin oxide nanocrystal-incorporated plasmonic gap-antennas and found a doubling of the third-harmonic conversion efficiency when comparing the third-harmonic response of the hybrid antennas to bare gold gap-antennas without indium tin oxide nanocrystals. However, a thorough study of bare and hybrid antennas revealed that the origin of the enhanced third-harmonic signal is located in the gold volume of the antennas rather than in the volume of the dielectric nanocrystals and is caused by an enhanced near-field of the red-shifted hybrid plasmonic gap-antennas.

Although many aspects of the nonlinear optical response of the plasmonic nanostructures investigated in this Review are well understood, there are still a number of unanswered questions. As an example, we investigated the second-harmonic response of dipole nanoantennas resonant to the second-harmonic wavelength and observed a strong enhancement of the second-harmonic emission. However, it has not been answered conclusively what the source of the second-harmonic signal is at all. The dipole nanoantennas are inversion symmetric structures and therefore should exhibit no second-order response.[13] There are different possible mechanisms that might explain the occurrence of the second-harmonic: One reason might be the symmetry breaking at the interface of the antennas or the substrate, or different electric near-field components might drive tensor elements that are not accessible from the far-field and that are not forbidden by symmetry. Also higher order magnetic dipole or electric quadrupole tensor elements might contribute to the second-harmonic signal. These higher order contributions become important as the nanostructure size becomes comparable to the wavelength of light.[9] A related question is whether deliberate symmetry breaking using asymmetric or chiral plasmonic structures allows further boosting the second-order response.[73−75]

Beyond that, in our experiments on hybrid plasmonic gap-antennas we did not observe a distinct third-harmonic signal from the dielectric indium tin oxide nanocrystals when compared to the third-harmonic signal that was emitted from the gold nanoantennas. The reason for the weak contribution of the indium tin oxide nanocrystals to the overall third-harmonic signal can be attributed to their weak third-order susceptibility when compared to the optical nonlinearity of gold. However, the overall concept is still promising. We believe that other nonlinear optical materials with higher third-order susceptibilities, such as semiconductors or nonlinear polymers, should give a distinct contribution to the overall TH response when incorporated into the hot-spot of plasmonic nanoantennas. Indeed there are few examples of mixed systems where the enhanced near-field of a plasmonic nanostructure drives the nonlinearity of a surrounding medium.[30−32] Hence, this concept might in the future lead to superior conversion efficiencies of nonlinear optical effects at the nanoscale.

DOI: 10.1021/acsphotonics.5b00587
ACS Photonics 2016, 3, 1336−1350

AUTHOR INFORMATION

Corresponding Author

*E-mail: giessen@physik.uni-stuttgart.de.

Notes

The authors declare no competing financial interest.

ACKNOWLEDGMENTS

We gratefully acknowledge financial support from the DFG (SPP1391, ultrafast nanooptics), from the Baden-Württemberg Stiftung (Kompetenznetz Funktionelle Nanostrukturen), from the BMBF (13N10146), and the ERC (Complexplas). The authors would like to thank Thorsten Schumacher, Markus Lippitz, Lili Gui, Jaco Fuchs, Dominik Floess, Xingchen Ye, Christopher B. Murray, Bastian Knabe, and Karsten Buse for collaborations as well as Sven Hein for graphical illustrations.

REFERENCES

(1) Metzger, B.; Hentschel, M.; Lippitz, M.; Giessen, H. Third-harmonic spectroscopy and modeling of the nonlinear response of plasmonic nanoantennas. *Opt. Lett.* **2012**, *37*, 4741−4743.

(2) Metzger, B.; Schumacher, T.; Hentschel, M.; Lippitz, M.; Giessen, H. Third Harmonic Mechanism in Complex Plasmonic Fano Structures. *ACS Photonics* **2014**, *1*, 471−476.

(3) Metzger, B.; Hentschel, M.; Schumacher, T.; Lippitz, M.; Ye, X.; Murray, C. B.; Knabe, B.; Buse, K.; Giessen, H. Doubling the Efficiency of Third Harmonic Generation by Positioning ITO Nanocrystals into the Hot-Spot of Plasmonic Gap-Antennas. *Nano Lett.* **2014**, *14*, 2867−2872.

(4) Metzger, B.; Gui, L.; Fuchs, J.; Floess, D.; Hentschel, M.; Giessen, H. Strong Enhancement of Second Harmonic Emission by Plasmonic Resonances at the Second Harmonic Wavelength. *Nano Lett.* **2015**, *15*, 3917−3922.

(5) Schuller, J. A.; Barnard, E. S.; Cai, W.; Jun, Y. C.; White, J. S.; Brongersma, M. L. Plasmonics for extreme light concentration and manipulation. *Nat. Mater.* **2010**, *9*, 193−204.

(6) Novotny, L.; van Hulst, N. Antennas for light. *Nat. Photonics* **2011**, *5*, 83−90.

(7) Liu, N.; Tang, M. L.; Hentschel, M.; Giessen, H.; Alivisatos, A. P. Nanoantenna-enhanced gas sensing in a single tailored nanofocus. *Nat. Mater.* **2011**, *10*, 631−636.

(8) Muehlschlegel, P.; Eisler, H.-J.; Martin, O. J. F.; Hecht, B.; Pohl, D. W. Resonant optical antennas. *Science* **2005**, *308*, 1607−1609.

(9) Kreibig, U.; Vollmer, M. *Optical Properties of Metal Clusters*; Springer, 1995.

(10) Bohren, C. F.; Huffman, D. R. *Absorption and Scattering of Light by Small Particles*; Wiley-Interscience Publication, 1998.

(11) Novotny, L.; Hecht, B. *Principles of Nano-Optics*; Cambridge University Press, 2006.

(12) Maier, S. A. *Plasmonics: Fundamentals and Applications*; Springer, 2007.

(13) Boyd, R. W. *Nonlinear Optics*, 3rd ed.; Academic Press, Elsevier, 2008.

(14) Kauranen, M.; Zayats, A. V. Nonlinear plasmonics. *Nat. Photonics* **2012**, *6*, 737−748.

(15) Klein, M. W.; Enkrich, C.; Wegener, M.; Linden, S. Second-Harmonic Generation from Magnetic Metamaterials. *Science* **2006**, *313*, 502−504.

(16) Lippitz, M.; van Dijk, M. A.; Orrit, M. Third-Harmonic Generation from Single Gold Nanoparticles. *Nano Lett.* **2005**, *5*, 799−802.

(17) Thyagarajan, K.; Rivier, S.; Lovera, A.; Martin, O. J. F. Enhanced second-harmonic generation from double resonant plasmonic antennae. *Opt. Express* **2012**, *20*, 12860−12865.

(18) Celebrano, M.; Wu, X.; Baselli, M.; Grossmann, S.; Biagioni, P.; Locatelli, A.; De Angelis, C.; Cerullo, G.; Osellame, R.; Hecht, B.; Duo, L.; Ciccacci, F.; Finazzi, M. Mode matching in multiresonant plasmonic nanoantennas for enhanced second harmonic generation. *Nat. Nanotechnol.* **2015**, *10*, 412−417.

(19) Linnenbank, H.; Linden, S. Second harmonic generation spectroscopy on second harmonic resonant plasmonic metamaterials. *Optica* **2015**, *2*, 698−701.

(20) Linnenbank, H.; Grynko, Y.; Foerstner, J.; Linden, S. Second harmonic generation spectroscopy on hybrid plasmonic/dielectric nanoantennas. *Light: Sci. Appl.* **2016**, *5*, e16013.

(21) Aouani, H.; Navarro-Cia, M.; Rahmani, M.; Sidiropoulos, T. P. H.; Hong, M.; Oulton, R. F.; Maier, S. A. Multiresonant Broadband Optical Antennas As Efficient Tunable Nanosources of Second Harmonic Light. *Nano Lett.* **2012**, *12*, 4997−5002.

(22) O'Brien, K.; Suchowski, H.; Rho, J.; Salandrino, A.; Kante, B.; Yin, X.; Zhang, X. Predicting nonlinear properties of metamaterials from the linear response. *Nat. Mater.* **2015**, *14*, 379−383.

(23) Harutyunyan, H.; Volpe, G.; Quidant, R.; Novotny, L. Enhancing the Nonlinear Optical Response Using Multifrequency Gold-Nanowire Antennas. *Phys. Rev. Lett.* **2012**, *108*, 217403.

(24) Lamprecht, B.; Krenn, J.; Leitner, A.; Aussenegg, F. Particle-plasmon decay-time determination bymeasuring the optical near-field's autocorrelation: influence of inhomogeneous line broadening. *Appl. Phys. B: Lasers Opt.* **1999**, *69*, 223−227.

(25) Hanke, T.; Cesar, J.; Knittel, V.; Trügler, A.; Hohenester, U.; Leitenstorfer, A.; Bratschitsch, R. Tailoring spatiotemporal light confinement in single plasmonic nanoantennas. *Nano Lett.* **2012**, *12*, 992−996.

(26) Luk'yanchuk, B.; Zheludev, N. I.; Maier, S. A.; Halas, N. J.; Nordlander, P.; Giessen, H.; Chong, C. T. The Fano resonance in plasmonic nanostructures and metamaterials. *Nat. Mater.* **2010**, *9*, 707−715.

(27) Butet, J.; Martin, O. J. F. Fano resonances in the nonlinear optical response of coupled plasmonic nanostructures. *Opt. Express* **2014**, *22*, 29693−29707.

(28) Zhang, Y.; Wen, F.; Zhen, Y.-R.; Nordlander, P.; Halas, N. J. Coherent Fano resonances in a plasmonic nanocluster enhance optical four-wave mixing. *Proc. Natl. Acad. Sci. U. S. A.* **2013**, *110*, 9215−9219.

(29) Thyagarajan, K.; Butet, J.; Martin, O. J. F. Augmenting Second Harmonic Generation Using Fano Resonances in Plasmonic Systems. *Nano Lett.* **2013**, *13*, 1847−1851.

(30) Chen, K.; Durak, C.; Heflin, J. R.; Robinson, H. D. Plasmon-Enhanced Second-Harmonic Generation from Ionic Self-Assembled Multilayer Films. *Nano Lett.* **2007**, *7*, 254−258.

(31) Niesler, F. B. P.; Feth, N.; Linden, S.; Niegemann, J.; Gieseler, J.; Busch, K.; Wegener, M. Second-harmonic generation from split-ring resonators on a GaAs substrate. *Opt. Lett.* **2009**, *34*, 1997−1999.

(32) Lee, J.; Tymchenko, M.; Argyropoulos, C.; Chen, P. Y.; Lu, F.; Demmerle, F.; Boehm, G.; Amann, M. C.; Alu, A.; Belkin, M. A. Giant nonlinear response from plasmonic metasurfaces coupled to intersubband transitions. *Nature* **2014**, *511*, 65−69.

(33) Canfield, B. K.; Husu, H.; Laukkanen, J.; Bai, B.; Kuittinen, M.; Turunen, J.; Kauranen, M. Local field asymmetry drives second-harmonic generation in non-centrosymmetric nanodimers. *Nano Lett.* **2007**, *7*, 1251−1255.

(34) Czaplicki, R.; Husu, H.; Siikanen, R.; Mäkitalo, J.; Kauranen, M.; Laukkanen, J.; Lehtolahti, J.; Kuittinen, M. Enhancement of Second-Harmonic Generation from Metal Nanoparticles by Passive Elements. *Phys. Rev. Lett.* **2013**, *110*, 093902.

(35) Linden, S.; Niesler, F. B. P.; Förstner, J.; Grynko, Y.; Meier, T.; Wegener, M. Collective Effects in Second-Harmonic Generation from Split-Ring-Resonator Arrays. *Phys. Rev. Lett.* **2012**, *109*, 1.

(36) Neira, A. D.; Olivier, N.; Nasir, M. E.; Dickson, W.; Wurtz, G. A.; Zayats, A. V. Eliminating material constraints for nonlinearity with plasmonic metamaterials. *Nat. Commun.* **2015**, *6*, 775710.1038/ncomms8757.

(37) Valev, V. K.; et al. Nonlinear superchiral meta-surfaces: tuning chirality and disentangling non-reciprocity at the nanoscale. *Adv. Mater.* **2014**, *26*, 4074−4081.

DOI: 10.1021/acsphotonics.5b00587
ACS Photonics 2016, 3, 1336−1350

(38) Li, Z.; Yao, K.; Xia, F.; Shen, S.; Tian, J.; Liu, Y. Graphene Plasmonic Metasurfaces to Steer Infrared Light. *Sci. Rep.* **2015**, *5*, 12423.
(39) Luo, L.; Chatzakis, I.; Wang, J.; Niesler, F. B.; Wegener, M.; Koschny, T.; Soukoulis, C. M. Broadband terahertz generation from metamaterials. *Nat. Commun.* **2014**, *5*, 3055.
(40) Mesch, M.; Metzger, B.; Hentschel, M.; Giessen, H. Nonlinear Plasmonic Sensing. *Nano Lett.* **2016**, *16*, 3155.
(41) Novotny, L. Effective Wavelength Scaling for Optical Antennas. *Phys. Rev. Lett.* **2007**, *98*, 266802.
(42) Sönnichsen, C.; Franzl, T.; Wilk, T.; von Plessen, G.; Feldmann, J.; Wilson, O.; Mulvaney, P. Drastic reduction of plasmon damping in gold nanorods. *Phys. Rev. Lett.* **2002**, *88*, 077402.
(43) Hentschel, M.; Utikal, T.; Giessen, H.; Lippitz, M. Quantitative Modelling of the Third Harmonic Emission Spectrum of Plasmonic Nanoantennas. *Nano Lett.* **2012**, *12*, 3778−3782.
(44) Stockman, M. I. Dark-hot resonances. *Nature* **2010**, *467*, 541.
(45) Gallinet, B.; Martin, O. J. F. Relation between near-field and far-field properties of plasmonic Fano resonances. *Opt. Express* **2011**, *19*, 22167−22175.
(46) Zhang, S.; Genov, D. A.; Wang, Y.; Liu, M.; Zhang, X. Plasmon-induced transparency in metamaterials. *Phys. Rev. Lett.* **2008**, *101*, 047401.
(47) Liu, N.; Langguth, L.; Weiss, T.; Kästel, J.; Fleischhauer, M.; Pfau, T.; Giessen, H. Plasmonic analogue of electromagnetically induced transparency at the Drude damping limit. *Nat. Mater.* **2009**, *8*, 758−762.
(48) Liu, N.; Weiss, T.; Mesch, M.; Langguth, L.; Eigenthaler, U.; Hirscher, M.; Sönnichsen, C.; Giessen, H. Planar Metamaterial Analogue of Electromagnetically Induced Transparency for Plasmonic Sensing. *Nano Lett.* **2010**, *10*, 1103−1107.
(49) Metzger, B.; Steinmann, A.; Hoos, F.; Pricking, S.; Giessen, H. Compact laser source for high-power white-light and widely tunable sub 65 fs laser pulses. *Opt. Lett.* **2010**, *35*, 3961−3963.
(50) Metzger, B.; Steinmann, A.; Giessen, H. High-power widely tunable sub-20 fs Gaussian laser pulses for ultrafast nonlinear spectroscopy. *Opt. Express* **2011**, *19*, 24354−24360.
(51) Niesler, F. B. P.; Feth, N.; Linden, S.; Wegener, M. Second-harmonic optical spectroscopy on split-ring-resonator arrays. *Opt. Lett.* **2011**, *36*, 1533−1535.
(52) Feynman, R. P.; Leighton, R. B.; Sands, M. *The Feynman Lectures on Physics*, vol. *1*; Addison-Wesley, 1997, 2007; Formula 30.19.
(53) Zuloaga, J.; Nordlander, P. On the redshift of the plasmonic near-field with respect to the far-field spectrum. *Nano Lett.* **2011**, *11*, 1280−1283.
(54) Demtröder, W. *Experimentalphysik2: Elektrizität und Optik*, 5th ed.; Springer, 2009.
(55) Johnson, P. B.; Christy, R. W. Optical Constants of the Noble Metals. *Phys. Rev. B* **1972**, *6*, 4370−4379.
(56) Knight, M. W.; Liu, L.; Wang, Y.; Brown, L.; Mukherjee, S.; King, N. S.; Everitt, H. O.; Nordlander, P.; Halas, N. J. Aluminum Plasmonic Nanoantennas. *Nano Lett.* **2012**, *12*, 6000−6004.
(57) McPeak, K. M.; Jayanti, S. V.; Kress, S. J. P.; Meyer, S.; Iotti, S.; Rossinelli, A.; Norris, D. J. Plasmonic Films Can Easily Be Better: Rules and Recipes. *ACS Photonics* **2015**, *2*, 326−333.
(58) Decker, M.; Feth, N.; Soukoulis, C. M.; Linden, S.; Wegener, M. Retarded long-range interaction in split-ring-resonator square arrays. *Phys. Rev. B: Condens. Matter Mater. Phys.* **2011**, *84*, 085416.
(59) Raschke, M. B.; Berweger, S.; Atkin, J. M. *Plasmonics: Theory and Applications*; Springer, 2014; Chapter Ultrafast and Nonlinear Plasmon Dynamics.
(60) Taubert, R.; Hentschel, M.; Kästel, J.; Giessen, H. Classical Analogue of Electromagnetically Induced Absorption in Plasmonics. *Nano Lett.* **2012**, *12*, 1367−1371.
(61) Klein, M. W.; Tritschler, T.; Wegener, M.; Linden, S. Lineshape of harmonic generation by metallic nanoparticles and metallic photonic crystal slabs. *Phys. Rev. B: Condens. Matter Mater. Phys.* **2005**, *72*, 115113.
(62) Utikal, T.; Zentgraf, T.; Kuhl, J.; Giessen, H. Dynamics and dephasing of plasmon polaritons in metallic photonic crystal superlattices: Time- and frequency-resolved nonlinear autocorrelation measurements and simulation. *Phys. Rev. B: Condens. Matter Mater. Phys.* **2007**, *76*, 245107.
(63) Utikal, T.; Zentgraf, T.; Paul, T.; Rockstuhl, C.; Lederer, F.; Lippitz, M.; Giessen, H. Towards the origin of the nonlinear response in hybrid plasmonic systems. *Phys. Rev. Lett.* **2011**, *106*, 133901.
(64) Feynman, R.; Leighton, R. B.; Sands, M. *Feynman Lectures on Physics*, Vol. *1*; Addison-Wesley, 1977; Formula 30.19.
(65) Dregely, D.; Neubrech, F.; Duan, H.; Vogelgesang, R.; Giessen, H. Vibrational near-field mapping of planar and buried three-dimensional plasmonic nanostructures. *Nat. Commun.* **2013**, *4*, 2237.
(66) Liu, N.; Guo, H.; Fu, L.; Kaiser, S.; Schweizer, H.; Giessen, H. Three-dimensional photonic metamaterials at optical frequencies. *Nat. Mater.* **2008**, *7*, 31−37.
(67) Black, C. T.; Murray, C. B.; Sandstrom, R. L. Embedded Nanoparticle Films and Method for Their Formation in Selective Areas on a Surface. US Patent US8465829 B2, 2013.
(68) Saboktakin, M.; Ye, X.; Chettiar, U. K.; Engheta, N.; Murray, C. B.; Kagan, C. R. Plasmonic Enhancement of Nanophosphor Upconversion Luminescence in Au Nanohole Arrays. *ACS Nano* **2013**, *7*, 7186−7192.
(69) Choi, S.; Nam, K. M.; Park, B. K.; Seo, W. S.; Park, J. T. Preparation and Optical Properties of Colloidal, Monodisperse, and Highly Crystalline ITO Nanoparticles. *Chem. Mater.* **2008**, *20*, 2609−2611.
(70) Alonso-González, P.; Albella, P.; Neubrech, F.; Huck, C.; Chen, J.; Golmar, F.; Casanova, F.; Hueso, L. E.; Pucci, A.; Aizpurua, J.; Hillenbrand, R. Experimental Verification of the Spectral Shift between Near- and Far-Field Peak Intensities of Plasmonic Infrared Nanoantennas. *Phys. Rev. Lett.* **2013**, *110*, 203902.
(71) http://refractiveindex.info.
(72) Aouani, H.; Rahmani, M.; Navarro-Cía, M.; Maier, S. A. Third-harmonic-upconversion enhancement from a single semiconductor nanoparticle coupled to a plasmonic antenna. *Nat. Nanotechnol.* **2014**, *9*, 290−294.
(73) Hentschel, M.; Schäferling, M.; Weiss, T.; Liu, N.; Giessen, H. Three-Dimensional Chiral Plasmonic Oligomers. *Nano Lett.* **2012**, *12*, 2542−2547.
(74) Yin, X.; Schäferling, M.; Metzger, B.; Giessen, H. Interpreting Chiral Nanophotonic Spectra: The Plasmonic Born−Kuhn Model. *Nano Lett.* **2013**, *13*, 6238−6243.
(75) Huttunen, M. J.; Bautista, G.; Decker, M.; Linden, S.; Wegener, M.; Kauranen, M. Nonlinear chiral imaging of subwavelength-sized twisted-cross gold nanodimers. *Opt. Mater. Express* **2011**, *1*, 46−56.

DOI: 10.1021/acsphotonics.5b00587
ACS Photonics 2016, 3, 1336−1350